Prevascularization of 3D printed bone scaffolds by bioactive hydrogels and cell co-culture

Mitchell Kuss

Shaohua Wu

Ying Wang

Jason B. Untrauer

Wenlong Li

See next page for additional authors

Authors

Mitchell Kuss, Shaohua Wu, Ying Wang, Jason B. Untrauer, Wenlong Li, Jung Yul Lim, and Bin Duan

Prevascularization of 3D printed bone scaffolds by bioactive hydrogels and cell co-culture

Mitchell A. Kuss[1,2], **Shaohua Wu**[1,2], **Ying Wang**[1,2], **Jason B. Untrauer**[3], **Wenlong Li**[4], **Jung Yul Lim**[1,4], **Bin Duan**[1,2,5]

[1]Mary and Dick Holland Regenerative Medicine Program, University of Nebraska Medical Center, Omaha, Nebraska

[2]Division of Cardiology, Department of Internal Medicine, University of Nebraska Medical Center, Omaha, Nebraska

[3]Division of Oral and Maxillofacial Surgery, Department of Surgery, College of Medicine, University of Nebraska Medical Center, Omaha, Nebraska

[4]Department of Mechanical and Materials Engineering, University of Nebraska-Lincoln, Lincoln, Nebraska

[5]Department of Surgery, College of Medicine, University of Nebraska Medical Center, Omaha, Nebraska

Abstract

Vascularization is a fundamental prerequisite for large bone construct development and remains one of the main challenges of bone tissue engineering. Our current study presents the combination of 3D printing technique with a hydrogel-based prevascularization strategy to generate prevascularized bone constructs. Human adipose derived mesenchymal stem cells (ADMSC) and human umbilical vein endothelial cells (HUVEC) were encapsulated within our bioactive hydrogels, and the effects of culture conditions on *in vitro* vascularization were determined. We further generated composite constructs by forming 3D printed polycaprolactone/hydroxyapatite scaffolds coated with cell-laden hydrogels and determined how the co-culture affected vascularization and osteogenesis. It was demonstrated that 3D co-cultured ADMSC-HUVEC generated capillary-like networks within the porous 3D printed scaffold. The co-culture systems promoted *in vitro* vascularization, but had no significant effects on osteogenesis. The prevascularized constructs were subcutaneously implanted into nude mice to evaluate the *in vivo* vascularization capacity and the functionality of engineered vessels. The hydrogel systems facilitated microvessel and lumen formation and promoted anastomosis of vascular networks of human origin with host murine vasculature. These findings demonstrate the potential of prevascularized 3D printed scaffolds with anatomical shape for the healing of larger bone defects.

Correspondence to: B. Duan; bin.duan@unmc.edu.

Additional Supporting Information may be found in the online version of this article.

INTRODUCTION

Bone grafts are commonly used for the treatment of acquired and congenital bone defects resulting from tumor resections, trauma, infections, cysts, and bone clefts.[1,2] >500,000 bone grafting procedures are performed annually in the United States, with a cost of over $2.5 billion.[3] Currently, the gold standard is autogenous bone, however, allogenic and xenogenic bone grafts are commonly used as well.[4] Limitations in bone graft volume, donor site morbidity, potential for disease transmission, and inconsistent integration with the host tissue are all potential drawbacks to bone grafting.[2]

Bone tissue engineering (BTE) holds the promise to enhance bone formation and regeneration by harnessing innovative scaffolds, stem cells, and biological factors.[5,6] Traditionally, BTE focused more on scaffold fabrication, stem cell differentiation, and growth factor release. However, more evidence has shown that the lack of vascularization within the engineered bone grafts can inhibit osteogenesis and host integration, thus inhibiting the healing of large bone defects.[7,8] Several strategies have been explored *in vitro* and *in vivo* for generating vascularized bone grafts, including growth factors or other biochemical angiogenic stimulation,[2,9] dynamic culture,[10] co-culture of endothelial cells with mesenchymal stem cells (MSC),[11,12] *in vivo* arteriovenous loops[13,14] and immunomodulation of adaptive immune cells.[15] The survival and function of engineered bone constructs after subsequent implantation is highly reliant on the speed in which they can develop adequate vascularization.[16,17] This is why increasing BTE efforts are needed to develop advanced bone scaffolds in parallel with the innovations in vascular tissue engineering.[13]

Another important aspect for BTE is to control the scaffold properties and fabrication. Among various bone tissue engineered scaffold fabrication techniques, 3D printing is a particularly promising technology.[18,19] 3D printing (or addictive manufacturing) employs automatic fabrication processes and thermoplastic biomaterials, like polycaprolactone (PCL). It enables the creation of 3D scaffolds with controllable pore size, porosity, and internal architecture in a layer-by-layer manner.[20,21] Importantly, 3D printing techniques can implement imaging techniques like computed tomography (CT) and magnetic resonance imaging (MRI) to generate patient specific 3D tissue models.[22,23] This will provide a blueprint for fabricating customized bone scaffolds with accurate anatomical shapes to fill the defect sites.

Therefore, combining 3D printed bone scaffolds with prevascularization strategies could ensure the appropriate size and shape of the forming bone, as well as the establishment of a vascular supply throughout the graft. Some efforts have been made to achieve this goal. Wang et al. subcutaneously implanted 3D printed porous poly(propylene fumarate) (PPF) scaffolds with a variety of combinations of pore sizes and porosities in a rat model to

evaluate vascular ingrowth and angiogenesis.[24] The *in silico* model demonstrated that vascularization decreases with increasing pore size (from 200 to 800 μm, with constant porosity) or increasing wall thickness. However, acellular scaffolds without any growth factor or physical stimuli cannot be fully vascularized. Mao's group integrated Arg-Gly-Asp (RGD)-phage nanofibers into the pores of 3D printed biphasic calcium phosphate scaffolds to induce the regeneration of vascularized bone *in vivo*.[25] The RGD-phage can regulate the endothelial cell (EC) migration and adhesion to induce endothelialization, while simultaneously activating osteoblastic differentiation of MSC. Mishra and co-workers developed a composite scaffold system of a 3D printed PPF shell and fibrin hydrogel with an MSC/human umbilical vein endothelial cell (HUVEC) spheroid.[26] Prevascularization conditioning shortened the neovascularization process, while the presence of the MSC/HUVEC spheroid assisted vascular infusion. However, single MSC/HUVEC spheroids resulted in uneven vasculature and rarely formed the complete vascularization needed for a larger bone defect. These methods for producing prevascularization in bone scaffolds need to be expanded on.

In our current study, we first encapsulated human adipose derived MSC (ADMSC) and HUVEC within chemically functionalized bioactive hydrogels consisting of hyaluronic acid (HA) and gelatin and co-cultured the constructs in hybrid media (consisting of growth medium for ADMSC and endothelial cell medium). Then, ADMSC-HUVEC laden hydrogels were formed around 3D printed PCL/hydroxyapatite (HAp) scaffolds and conditioned in hybrid media for 3 weeks to assess the effects of co-culture on vascularization and ADMSC osteogenic differentiation within the constructs. We further implanted bone constructs subcutaneously into athymic mice to determine the EC-MSC interactions *in vivo* and compared functionality of engineered vessels in various scaffolds.

MATERIALS AND METHODS

Cell culture and differentiation

Established primary human ADMSC were purchased from Lonza and cultured in growth medium (GM) containing DMEM/F12 medium (Invitrogen), 10% FBS (Invitrogen) and 1% P/S (Invitrogen). For osteogenic differentiation, osteogenic medium (OGM) consisted of GM, 100 nM dexamethasone (Sigma), 10 mM β-glycerophosphate (Sigma) and 50 μM ascorbic acid (Sigma).[27] HUVEC (Lonza) were grown in EGM (EGM-2 BulletKit, Lonza) used until passage 6. The cells were cultured in 5% CO_2 at 37°C. ADMSC or ADMSC/HUVEC spheroids were prepared by the hanging drop method. Briefly, 20 μL of cell resuspension (ADMSC, or ADMSC: HUVEC = 1:1), with a density of 5×10^6 cells/ml was placed onto the lid of 48-well plate and cultured overnight.

Polymer modification and hydrogel preparation

Photocrosslinkable HA (NovaMatrix, fermented from Streptococcus zooepidemicus, ~1200 kDa) and gelatin (Type B from bovine skin, Sigma) were synthesized as previously reported[28] through the reaction of methacrylic anhydride (Sigma) with 0.5% HA or 10% gelatin in deionized water. For hydrogel preparation, methacrylated HA (Me-HA), 0.75%w/v and methacrylated gelatin (Me-Gel), 1.5%w/v were dissolved in cell culture

medium with 0.05% w/v 2-hydroxy-1(4-(hydroxyethox)phenyl)-2-methyl-1-propanone (Irgacure 2959; CIBA Chemicals) and homogeneous cell suspension [totally 4×10^6 cells/ml, ADMSC:HUVEC = 1:1, Figure 1(A)] or cell spheroid encapsulation [Figure 1(B)]. The hydrogel precursor was transferred into silicone molds (8 mm in diameter, 1 mm in thickness, for cell and spheroid encapsulation) and subsequently exposed to OmniCure S2000 UV lamp (Lumen Dynamics, 365 nm) for 60 s at room temperature.

3D printing and scaffold characterization

PCL/HAp nanocomposite scaffolds were 3D printed using the 3D Bioplotter (EnvisionTEC, Germany). PCL pellets (Sigma, Mw = 65,000) and HAp nanocrystal (100 nm, Berkeley Advacned Biomaterials, Inc; 10% of PCL,) were air dried at 37°C overnight and then loaded in the stainless steel syringe with 22 G metal tip and heated at a temperature of 140°C for 10 min. As PCL reached the molten phase, the temperature was maintained at 120°C during printing. A pressure of 3–3.5 bar was applied to the syringe and deposition speed of 1.8–2.2 mm/s was used. 3D cylinder scaffold (8 mm in diameter and 2 mm in thickness) was designed using VisualMachines software (EnvisionTEC), and the design file was loaded into the 3D printer. PCL/HAp was deposited at different angles (0° and 90°) between two successive layers. A scanning electron microscope (SEM, FEI Quanta 200) was used to characterize surface morphology of 3D printed PCL/HAp scaffolds. The uniaxial compression testing of PCL and PCL/HAp was conducted using an MTS machine (INSTRON 8500 Plus, 25 KN) at a loading rate of 0.015 mm/s at room temperature. Before cell encapsulation or cell seeding, the 3D printed PCL/HAp scaffolds were disinfected in 70% (v/v) ethanol overnight, and then were incubated in GM overnight, after being washed in phosphate buffered saline solution (PBS). For surface seeding, totally 8×10^5 cells (ADMSC:HUVEC = 1:1) were suspended in 200 μL hybrid medium and were seeded onto the PCL/HAp scaffolds. ADMSC or ADMSC plus HUVEC (1:1) with the same cell density were encapsulated within the hydrogel, then the hydrogel with cells (200 μL) was deposited around the printed PCL/HAp scaffolds, allowing it to settle into the scaffold before UV crosslinking in the manner mentioned above in Section 2.2 [Figure 1(C)]. After cell seeding or encapsulation, the constructs were cultured in hybrid media with OGM and EGM (OGM: EGM = 1:1) for 21 days.

Alkaline phosphatase (ALP) staining and activity

Alkaline phosphatase leukocyte kit (Sigma) was used according to the manufacturer's protocol for ALP staining. ALP activity quantification was performed as previously described.[28] Briefly, the lysed cells were mixed with ALP substrate solution containing p-nitrophenyl phosphate (pNPP) (Sigma) at 37°C for 25 min. The reaction was stopped by the addition of NaOH, then the production of p-nitrophenol in the presence of ALPase was measured by monitoring the absorbance of the solution at a wavelength of 405 nm using a microplate reader (Bio-Tek Instruments). The total protein content was determined using a BCA assay kit (Pierce, Rockford, IL, USA) with bovine serum albumin as a standard, and the ALP activity was expressed as μmol of p-nitrophenol formation per minute per milligram of total proteins (μmol/min/mg protein).

RNA isolation and qPCR

Total RNA was extracted from the whole cell-laden constructs, without separating the co-cultured cells, using QIA-Shredder and RNeasy mini-kits (QIAgen), according to the manufacturer's instructions. Total RNA was synthesized into first strand cDNA in a 20 μL reaction using an iScript cDNA synthesis kit (BioRad Laboratories). Real-time PCR analysis was performed in a StepOnePlus™ Real-Time PCR System (Thermo Scientific) using SsoAdvanced SYBR Green Supermix (Bio-Rad). cDNA samples were analyzed for the gene of interest and for the housekeeping gene 18 S rRNA. The level of expression of each target gene was calculated using comparative Ct ($2^{-\Delta Ct}$) method.[28,29] All primers used in this study are listed in Supporting Information Table S1.

In vivo subcutanous implantation

Eight-week old, female athymic nude mice were purchased from Jackson Laboratory. The mice were housed in compliance with the University of Nebraska Medical Center (UNMC) guidelines. All surgery procedures were reviewed and approved by UNMC Animal Care and Use Committee. The cell laden constructs (scaffold with ADMSC encapsulation, scaffold with surface seeded ADMSC + HUVEC, and scaffold with ADMSC + HUVEC encapsulation) were conditioned in hybrid media (OGM + EGM) for 21 days, and then five samples of each group were subcutaneously implanted in the nude mice (two samples per mouse and 10 mice in total). The printed PCL/HAp scaffold alone served as control. For the surgery, the mice were deeply anesthetized, and one dorsal incision was made, lateral to the spine. Two subcutaneous pockets were made from this single incision, one on each side of the mouse, using blunt dissection. The scaffold implants were gently inserted into the subcutaneous pockets. The single skin incision was closed with wound clips, and the mice were monitored closely to ensure full recovery from anesthesia. All of the animals were sacrificed after 4-week implantation.

Histological and immunohistochemical staining

Cell-laden hydrogels were fixed in 4% paraformaldehyde, and printed PCL/HAp scaffolds with cells were fixed in 10% neutralized formalin overnight. The PCL/HAp scaffold samples were embedded in optimal cutting temperature (OCT) compound (Fisher Scientific) and cross-sectioned (~10 μm in thick) using a cryosectioner (Leica). H&E staining was conducted for implanted scaffolds. For immunohistochemical staining, the samples (hydrogels or sectioned slides) were permeabilized in 0.2% Triton X-100 then blocked with 1% bovine serum albumin (BSA) overnight at 4°C. The samples were incubated with primary antibodies to α-smooth muscle actin (αSMA) (1:200, Sigma) and/or anti-human specific CD31 (1:100, Cell Signaling) overnight at 4°C. Secondary fluorescent antibodies and/or Alexa Fluor 488-conjugated phalloidin (1:40, Invitrogen) were incubated for 2 h, and nuclear counterstaining (Draq 5, 1: 1000, Thermo Scientific) was performed for 30 min at room temperature. The stained samples were imaged with a Zeiss 710 CLSM.

Quantitative estimation of cell migration rate and microvessel density

The cell migration rate in spheroid encapsulated hydrogels was quantified by measuring the migration distance from the edge of the spheroids using Image J software (NIH). Three

independent spheroid encapsulations were performed for each group, and at least twenty distance measures were conducted for each image. Microvessel density and area within the constructs, after *in vivo* implantation, were calculated by using two images per sample from the images of five scaffold samples (totally, 10 images for each group). The microvessels were identified as luminal structures with CD31 positive cells, and microvessel areas were calculated by identifying and calculating CD31 (red) positive areas in each immunofluorescent staining image.

Statistical analysis

All quantitative data were expressed as mean ± standard deviation (SD). Pairwise comparisons between groups were conducted using ANOVA with Scheffé post-hoc tests in statistical analysis. A value of $p < 0.05$ was considered statistically significant.

RESULTS

3D co-culture of ADMSC and HUVEC within bioactive hydrogel

We first evaluated the morphology and gene expression of ADMSC and ADMSC-HUVEC co-culture (1:1 ratio) within bioactive hydrogels, consisting of Me-HA and Me-Gel, in different condition media, as shown in Figure 1(A). In GM, ADMSC alone only expressed alpha smooth muscle actin (αSMA) and were mostly negative for CD31, which is a marker for endothelial cells. [Figure 2(A)]. The addition of EGM significantly promoted the expression of vascularization related genes, like VEGFA, vWF and PECAM1 [Figure 2(B)], but ADMSC still expressed very limited CD31 in the hybrid media [Figure 2(A)]. For the co-culture system, obvious CD31 expression was observed, and the presence of ADMSC induced the HUVEC to form capillary-like structures [Figure 2(A)]. The expressions of VEGFA, vWF, and PECAM1 were upregulated by 69.2 ± 13.2 fold, 82.1 ± 13.5 fold, and 22.8 ± 12.5 fold, respectively.

We further generated ADMSC spheroids or ADMSC-HUVEC spheroids and encapsulated them into Me-HA/Me-Gel hydrogels to assess cell migration and sprouting [Figure 1(B)]. All of the cells showed obvious migration from spheroids after 7-day culture [Figure 3(A)]. We found that the addition of EGM did not affect the ADMSC migration compared to the GM condition [Figure 3(A, B)]. The co-culture of ADMSC-HUVEC promoted cell migration and sprouting from the spheroid and showed significantly higher migration distance [Figure 3(A,B)]. QPCR results showed that co-cultured spheroids expressed more MMP1, MMP2, and MMP12, indicating that the co-cultured cells had better matrix digestion capacity. These results were consistent with the migration test.

3D printed PCL/HAp scaffolds

Both PCL and PCL/HAp have been successfully 3D printed.[30–32] In our current study, we 3D printed PCL scaffolds with 10% HAp. The scaffold had regular pores of around 500 μm and strands with a thickness of 350–450 μm, based on light microscopy an SEM [Figure 4(A,B)]. All of the design and printing processes are controllable, and the PCL/HAp scaffolds were 3D printed with different patterns to control the porosity and mechanical properties (Supporting Information Figure S1). Most of the HAp particles were embedded

inside of the PCL polymer, rather than on the surface [Figure 4(C)], during the melting and extrusion process. The compressive modulus of the PCL scaffold was slightly higher than that of the PCL/HAp scaffold, but did not meet the level of statistical significance. [Figure 4(D)].

In vitro vascularization within 3D printed scaffolds

We 3D printed PCL/HAp scaffolds and encapsulated ADMSC or ADMSC-HUVEC within the Me-HA/Me-Gel hydrogel around PCL/HAp scaffolds [Figure 1(C)]. The whole constructs were conditioned in hybrid media with OGM and EGM. The cell-laden hydrogels remained intact around and inside the scaffolds through 21-day of culture. Similar to culture in gel alone, most ADMSC cultured in the composite scaffold did not express CD31 [Figure 5(A)]. On the printed scaffold surface, the co-cultured ADMSC-HUVEC cells became confluent after 21-day culture and stained positive for CD31 [Figure 5(A)]. The encapsulated HUVEC formed microvessel-like structures within the constructs. Gene expressions of VEGFA, PECAM1, CDH5, and vWF were all significantly upregulated in the co-cultured constructs [Figure 5(B)], but there was no significant difference between the ADMSC-HUVEC surface seeding group and the encapsulation group.

In vitro osteogenic differentiation of ADMSC-HUVEC co-culture in 3D printed scaffolds

Next, we evaluated the osteogenic ability of ADMSC and ADMSC-HUVEC to determine whether or not co-culturing affects osteogenic differentiation *in vitro*. All constructs stained positive for alkaline phosphatase (ALP), revealing that all the constructs expressed substantial ALP [Figure 6(A)]. Also, the ALP activity significantly increased with increasing culture time from day 7 to day 21 for all the three groups [Figure 6(B)], but there were no significant differences between different groups. QPCR results showed that surface seeded ADMSC-HUVEC expressed slightly more osteogenic differentiation markers (ALP, Runx2, OCN, and OPN), but no statistical difference was observed. These results indicate that the co-culture and the use of EGM did not affect the *in vitro* osteogenic differentiation of MSC.

In vivo formation of vascular networks and microvessel density

In order to determine the capacity of the vascular network formation within 3D printed PCL/HAp *in vivo*, we surgically implanted cell-laden constructs into immunodeficient mice for 4 weeks. Printed acellular scaffolds were used as the control. All of the cell-laden constructs were conditioned in hybrid media consisting of OGM and EGM for 21 days before implantation. Figure 7(A) shows the macroscopic views of different scaffolds after explantation. None of the constructs evoked noticeable host inflammatory response. The acellular PCL/HAp scaffold showed very limited blood vessel infiltration. In contrast, the scaffolds with ADMSC-HUVEC surface seeding and encapsulation showed extensive blood vessels along the channel areas. H&E staining in Figure 7(B) show that the acellular scaffolds were infiltrated with some host cells, while the scaffolds with encapsulated ADMSC showed small remnants of hydrogels (hollow arrows). Both ADMSC-HUVEC surface seeding and encapsulation scaffolds were densely populated with cells (both host cells and pre-seeded/encapsulated cells) throughout the samples [Figure 7(B)]. As indicated in Figure 3, the co-culture of ADMSC-HUVEC expressed more MMP1, 2, 12 and thus

remodeled the matrix more quickly. This is probably why the constructs were populated with more cells and less matrix. The scaffolds with encapsulated and surface seeded ADMSC-HUVEC showed extensive microvascularity. In addition, many murine erythrocytes [white narrow arrows, Figure 7(B)] were also observed within the microvessels, indicating the integration of formed lumens with existing host vasculature. The perfused microvasculature stained positive for human CD31, which was stained by human specific anti-CD31 antibody, suggesting that the cells along the lumens were of human origin. In contrast, there were significantly fewer CD31 positive microvessels within the scaffolds with ADMSC alone. Although H&E staining demonstrated some vascular structures in the acellular scaffold group, no obvious human CD31 positive microvessels were observed. This indicates that the microvasculatures observed in H&E staining were probably of mouse origin.

Quantification of the microvessel density and area distribution resulted in statistically significant differences among the three groups [Figure 7(D,E)]. The human CD-31 positive microvessel density was similar in the ADMSC-HUVEC surface seeding and encapsulation groups. This was significantly higher than in the ADMSC encapsulated scaffolds [Figure 7(D)]. There are probably multiple affecting factors, and one of the reasons is that the hydrogel could block the pores of the scaffold, which would affect the nutrition transportation and, to a certain degree, counteract their positive effects as vascular bed. The distribution of ingrowing neo-vessels seemed more homogeneous within the ADMSC-HUVEC surface seeded scaffolds [Figure 7(E)]. In the ADMSC-HUVEC encapsulated scaffolds, both median and average lumen sizes ($163.1 \pm 56.7~\mu m^2$ and $337.0 \pm 130.3~\mu m^2$) were significantly larger than those in the scaffolds with ADMSC ($83.3 \pm 16.2~\mu m^2$ and $146.0 \pm 42.3~\mu m^2$) or ADMSC-HUVEC surface seeding ($83.3 \pm 16.2~\mu m^2$ and $112.5 \pm 64.8~\mu m^2$).

DISCUSSION

Prevascularization has been shown to be a promising strategy to establish some vascular supply prior to implantation and to promote subsequent new bone formation.[7,33,34] Although 3D printed PCL/HAp scaffolds have been widely fabricated and used, most of them focused on the osteogenic differentiation of osteoblasts and MSC.[35,36] In our current study, we combined 3D printing with a co-culture of EC and MSC and focused on the capacity of osteogenic differentiation and vascularization of the constructs. We implemented bioactive hydrogels consisting of Me-HA and Me-Gel as cell carriers to encapsulate the co-cultured cells. We hypothesize that the incorporation of HUVEC facilitates the prevascularization in the 3D printed scaffolds and that the hydrogel encapsulated cells promote superior microvessel formation when compared to surface cell seeding. Our previous studies have demonstrated that Me-HA/Me-Gel hydrogels have tunable stiffnesses[37] and can be incorporated with conjugated growth factors.[27] Chen et al. reported that the extent of the vascular network formation was significantly altered by the degree of Me-Gel methacrylation which mainly affected the hydrogel stiffness.[38] We used Me-HA/Me-Gel hydrogels with relatively low level of stiffness (1.41 ± 0.27 kPa) in our study and demonstrated that the hydrogels supported the formation of capillary network structures.

The 3D printing techniques have been applied to generate clinically relevant geometries for accurately shaped bone reconstruction.[39–41] We implemented PCL/HAp composite materials and generated porous scaffolds, which have controllable patterns with the ability to replicate the complex defect anatomy of the mandible (Supporting Information Figure S1). HAp were mostly within the strands during the melting and printing process and had limited effects on mechanical properties and cell behavior. Larger amounts of HAp can be incorporated, and further surface modification can be conducted in future studies to improve the mineralization process. The porous printed scaffolds allowed for surface cell seeding and hydrogel encapsulation. The cell-laden macromer precursors can penetrate into the scaffolds and form uniform hydrogels around the printed PCL/HAp scaffolds after photocrosslink. Therefore, our composite scaffold system is composed of a mechanically robust porous matrix, which supports the maintenance of the bone defect and initial bone ingrowth, and a soft hydrogel, which supports vascular sprouting.

Co-culture of MSC and EC is commonly utilized for co-seeding on biologic scaffolds for bone regeneration.[42,43] Surface seeding may result in non-uniform cell distribution, especially for large bone grafts. Animal derived extracellular matrix (ECM) proteins, such as collagen and fibrin, are used as cell or growth factor carriers for cell encapsulation and growth factor delivery within porous bone scaffolds.[44,45] We implemented a more tunable Me-HA/Me-Gel hydrogel system for the cell encapsulation and directly compared the vascularization capacity with the surface seeded ADMSC and HUVEC. It is important to compare these strategies to better design and fabricate cell-laden scaffolds. Our results show that encapsulation within engineered vascular beds did not significantly upregulate vascularization gene expression, but did improve the microvessel formation *in vitro* and promoted larger and denser lumen formation that are of human origin. The formed microvascular vessels within the hydrogels were not only due to host blood vessel invasion, but also developed from the implanted human cells. In both ADMSC-HUVEC surface seeding and encapsulation groups, murine erythrocytes were observed within formed microvessels, indicating the functional integration with the host-murine vasculature.

The vascularization capacity of ADMSC remains unclear: some studies have shown that ADMSC alone can form microvascular structures *in vitro*,[45,46] while others have demonstrated that ADMSC alone have no effect, and may impair the vascularization when ADMSC were pre-differentiated into an osteogenic lineage.[47,48] The results of our current study show that ADMSC have a limited capacity to differentiate to CD31 positive EC and form capillary-like structures *in vitro* and *in vivo*. The angiogenic potential of ADMSC is mediated by matrix components,[49,50] topography,[51] pre-differentiation status,[52] and biochemical and biophysical stimuli.[47,53] In the co-culture system, many studies show that ADMSC can facilitate the vasculogenesis of EC *in vitro*[54,55]. Direct contact of EC and ADMSC is essential for mature vascular network formation, as ADMSC contribute to vessel stabilization by expressing the pericyte marker.[56] Our results also demonstrate that co-cultured ADMSC and HUVEC expressed more ECM degradation enzymes, which promote cell migration and capillary network formation.

The effect of co-culture on osteogenic differentiation is another important issue for BTE. Kim et al. reported that co-culture of MSC and HUVEC enhanced the osteogenic

differentiation of MSC in a 2 D culture, and that osteogenesis was further enhanced on the matrix with nanotopographic features.[57] In contrast, Meury et al. showed that HUVEC inhibited osteoblastic differentiation of MSC in OGM and hybrid medium.[58] In our current study, we demonstrate that co-culture of ADMSC and HUVEC, in both 2 D surface culture and 3D encapsulation, did not affect osteogenic differentiation of ADMSC compared to the ADMSC alone group. It has also been reported that the temporal variation of the culture environment and culture sequence might affect the osteogenesis and vascularization as well. [59,60] Development of vascularization prior to osteogenesis can better promote the osteogenic induction, thus suggesting that further effort should be made to synergize vascular development and osteogenesis. In the current study, we used hybrid media consisting EGM and OGM, and the sequential exposure to EGM and OGM was not adequately considered, which could create vessels and bone in their highest capacities after optimization of the best order and culture time. Future study will focus on determining how the prevascularization affects bone regeneration in a rabbit model with large craniofacial defect.

CONCLUSIONS

In our current study, we generated composite scaffolds consisting of 3D printed PCL/HAp and bioactive hydrogels for the prevascularization of engineered bone constructs. The co-culture of ADMSC and HUVEC promoted *in vitro* vascularization, cell migration, and sprouting, but did not significantly affect osteogenesis. The Me-HA/Me-Gel hydrogels provide an engineered vascular bed and facilitated the formation of microvessels and vasculatures with both human and mouse origin. Our strategy may help in prevascularization of patient specific constructs *in vitro* to achieve rapid anastomosis *in vivo* and enhance bone repair.

Supplementary Material

Refer to Web version on PubMed Central for supplementary material.

ACKNOWLEDGMENTS

REFERENCES

1. Griffin KS, Davis KM, McKinley TO, Anglen JO, Chu TMG, Boerckel JD, Kacena MA. Evolution of bone grafting: Bone grafts and tissue engineering strategies for vascularized bone regeneration. Clin Rev Bone Miner Metab 2015;13:232–244.

2. Samorezov JE, Alsberg E. Spatial regulation of controlled bioactive factor delivery for bone tissue engineering. Adv Drug Deliv Rev 2015;84:45–67. [PubMed: 25445719]

3. Giannoudis PV, Dinopoulos H, Tsiridis E. Bone substitutes: an update. Injury 2005;36:S20–27. [PubMed: 16188545]

4. Verrier S, Alini M, Alsberg E, Buchman SR, Kelly D, Laschke MW, Menger MD, Murphy WL, Stegemann JP, Schütz M, Miclau T, Stoddart MJ, Evans C. Tissue engineering and regenerative approaches to improving the healing of large bone defects. European Cells and Materials 2016;32:87–110. [PubMed: 27434267]

5. Bose S, Roy M, Bandyopadhyay A. Recent advances in bone tissue engineering scaffolds Trends Biotechnol 2012;30:546–554. [PubMed: 22939815]

6. Tsigkou O, Pomerantseva I, Spencer JA, Redondo PA, Hart AR, O'Doherty E, Lin Y, Friedrich CC, Daheron L, Lin CP, Sundback CA, Vacanti JP, Neville C. Engineered vascularized bone grafts Proc Natl Acad Sci U S A 2010;107:3311–3316. [PubMed: 20133604]

7. García JR, García AJ. Biomaterial-mediated strategies targeting vascularization for bone repair. Drug Deliv Transl Res 2016;6:77–95. [PubMed: 26014967]

8. Amini AR, Laurencin CT, Nukavarapu SP. Differential analysis of peripheral blood- and bone marrow-derived endothelial progenitor cells for enhanced vascularization in bone tissue engineering. J Orthop Res 2012;30:1507–1515. [PubMed: 22378621]

9. Hutton DL, Moore EM, Gimble JM, Grayson WL. Platelet-derived growth factor and spatiotemporal cues induce development of vascularized bone tissue by adipose-derived stem cells. Tissue Eng - Part A 2013;19:2076–2086. [PubMed: 23582144]

10. Santos MI, Reis RL. Vascularization in bone tissue engineering: Physiology, current strategies, major hurdles and future challenges. Macromol Biosci 2010;10:12–27. [PubMed: 19688722]

11. Kirkpatrick CJ, Fuchs S, Unger RE. Co-culture systems for vascularization - Learning from nature. Adv Drug Deliv Rev 2011;63: 291–299. [PubMed: 21281686]

12. Brennan MA, Davaine JM, Layrolle P. Pre-vascularization of bone tissue-engineered constructs. Stem Cell Res Ther 2013;4:96. [PubMed: 23953741]

13. Mercado-Pagán ÁE, Stahl AM, Shanjani Y, Yang Y. Vascularization in bone tissue engineering constructs. Ann Biomed Eng 2015;43:718–729. [PubMed: 25616591]

14. Dong QS, Shang H, Wu W, Chen FL, Zhang JR, Guo JP, Mao TQ. Prefabrication of axial vascularized tissue engineering coral bone by an arteriovenous loop: A better model. Mater Sci Eng C 2012; 32:1536–1541.

15. Spiller KL, Nassiri S, Witherel CE, Anfang RR, Ng J, Nakazawa KR, Yu T, Vunjak-Novakovic G. Sequential delivery of immunomodulatory cytokines to facilitate the M1-to-M2 transition of macrophages and enhance vascularization of bone scaffolds. Biomaterials 2015;37:194–207. [PubMed: 25453950]

16. Laschke MW, Menger MD. Prevascularization in tissue engineering: Current concepts and future directions. Biotechnol Adv 2016; 34:112–121. [PubMed: 26674312]

17. Sivaraj KK, Adams RH. Blood vessel formation and function in bone. Development 2016;143:2706–2715. [PubMed: 27486231]

18. Bose S, Vahabzadeh S, Bandyopadhyay A. Bone tissue engineering using 3D printing. Materials Today 2013;16:496–504.

19. Duan B, Cheung W, Wang M. Optimized fabrication of Ca-P/PHBV nanocomposite scaffolds via selective laser sintering for bone tissue engineering. Biofabrication 2011;3:015001. [PubMed: 21245522]

20. Inzana JA, Olvera D, Fuller SM, Kelly JP, Graeve OA, Schwarz EM, Kates SL, Awad HA. 3D printing of composite calcium phosphate and collagen scaffolds for bone regeneration. Biomaterials 2014;35:4026–4034. [PubMed: 24529628]

21. Duan B, Wang M. Selective laser sintering and its application in biomedical engineering. MRS Bull 2011;36:998–1005.

22. Murphy SV, Atala A. 3D bioprinting of tissues and organs. Nat Biotechnol 2014;32:773–785. [PubMed: 25093879]

23. Chia HN, Wu BM. Recent advances in 3D printing of biomaterials. J Biol Eng 2015;9:4. [PubMed: 25866560]

24. Wang MO, Vorwald CE, Dreher ML, Mott EJ, Cheng MH, Cinar A, Mehdizadeh H, Somo S, Dean D, Brey EM, Fisher JP. Evaluating 3D-printed biomaterials as scaffolds for vascularized bone tissue engineering. Adv Mater 2014;27:138–144. [PubMed: 25387454]

25. Wang J, Yang M, Zhu Y, Wang L, Tomsia AP, Mao C. Phage nanofibers induce vascularized osteogenesis in 3D printed bone scaffolds. Adv Mater 2014;26:4961–4966. [PubMed: 24711251]

26. Mishra R, Roux BM, Posukonis M, Bodamer E, Brey EM, Fisher JP, Dean D. Effect of prevascularization on in vivo vascularization of poly(propylene fumarate)/fibrin scaffolds. Biomaterials 2016;77:255–266. [PubMed: 26606451]

27. Duan B, Hockaday LA, Das S, Xu CY, Butcher JT. Comparison of mesenchymal stem cell source differentiation towards human pediatric aortic valve interstitial cells within 3D engineered matrices. Tissue Eng Part C Methods 2015;21:795–807. [PubMed: 25594437]

28. Duan B, Yin ZY, Kang LH, Magin RL, Butcher JT. Active tissue stiffness modulation controls valve interstitial cell phenotype and osteogenic potential in 3D culture. Acta Biomater 2016;36:42–54. [PubMed: 26947381]

29. Yuan JS, Reed A, Chen F, Stewart JCN. Statistical analysis of real-time PCR data. BMC Bioinformatics 2006;7:85. [PubMed: 16504059]

30. Shor L, Güçceri S, Wen X, Gandhi M, Sun W. Fabrication of three dimensional polycaprolactone/hydroxyapatite tissue scaffolds and osteoblast-scaffold interactions in vitro. Biomaterials 2007;28:5291–5297. [PubMed: 17884162]

31. Park SA, Lee SH, Kim WD. Fabrication of porous polycaprolactone/hydroxyapatite (PCL/HA) blend scaffolds using a 3D plotting system for bone tissue engineering. Bioprocess Biosyst Eng 2011; 34:505–513. [PubMed: 21170553]

32. Kang HW, Lee SJ, Ko IK, Kengla C, Yoo JJ, Atala A. A 3D bioprinting system to produce human-scale tissue constructs with structural integrity. Nat Biotechnol 2016;34:312–319. [PubMed: 26878319]

33. Chen X, Aledia AS, Ghajar CM, Griffith CK, Putnam AJ, Hughes CCW, George SC. Prevascularization of a fibrin-based tissue construct accelerates the formation of functional anastomosis with host vasculature. Tissue Eng - Part A 2009;15:1363–1371. [PubMed: 18976155]

34. Choi SW, Zhang Y, Macewan MR, Xia Y. Neovascularization in biodegradable inverse opal scaffolds with uniform and precisely controlled pore sizes. Adv Healthcare Mater 2013;2:145–154.

35. Goncalves EM, Oliveira FJ, Silva RF, Neto MA, Fernandes MH, Amaral M, Vallet-Regí M, Vila M. Three-dimensional printed PCL-hydroxyapatite scaffolds filled with CNTs for bone cell growth stimulation. J Biomed Mater Res B Appl Biomater 2016;104:1210–1219. [PubMed: 26089195]

36. Rumi ski S, Ostrowska B, Jaroszewicz J, Skirecki T, Włodarski K, wi szkowski W, Lewandowska-Szumieł M. 3D printed PCL-based scaffolds provide an advantageous environment for osteogenic differentiation of human adipose-derived stem cells. J Tissue Eng Regen Med 2016. DOI: 10.1002/term.2310.

37. Duan B, Hockaday LA, Kapetanovic E, Kang KH, Butcher JT. Stiffness and adhesivity control aortic valve interstitial cell behavior within hyaluronic acid based hydrogels. Acta Biomater 2013;9:7640–7650. [PubMed: 23648571]

38. Chen YC, Lin RZ, Qi H, Yang Y, Bae H, Melero-Martin JM, Khademhosseini A. Functional human vascular network generated in photocrosslinkable gelatin methacrylate hydrogels. Adv Funct Mater 2012;22:2027–2039. [PubMed: 22907987]

39. Duan B, Wang M. Customized Ca-P/PHBV nanocomposite scaffolds for bone tissue engineering: design, fabrication, surface modification and sustained release of growth factor. J R S Interface 2010;7:S615–S629.

40. Raja N, Yun HS. A simultaneous 3D printing process for the fabrication of bioceramic and cell-laden hydrogel core/shell scaffolds with potential application in bone tissue regeneration. J Mater Chem B 2016;4:4707–4716. [PubMed: 32263243]

41. Hung BP, Naved BA, Nyberg EL, Dias M, Holmes CA, Elisseeff JH, Dorafshar AH, Grayson WL. Three-dimensional printing of bone extracellular matrix for craniofacial regeneration. ACS Biomater Sci Eng 2016;2:1806–1816. [PubMed: 27942578]

42. Seebach C, Henrich D, Wilhelm K, Barker JH, Marzi I. Cell transplantation. Endothelial progenitor cells improve directly and indirectly early vascularization of mesenchymal stem cell-driven bone regeneration in a critical bone defect in rats 2012;21:1667–1677.

43. Koob S, Torio-Padron N, Stark GB, Hannig C, Stankovic Z, Finkenzeller G. Bone formation and neovascularization mediated by mesenchymal stem cells and endothelial cells in critical-sized calvarial defects. Tissue Eng - Part A 2011;17:311–321. [PubMed: 20799886]

44. Yang P, Huang X, Wang C, Dang X, Wang K. Repair of bone defects using a new biomimetic construction fabricated by adipose-derived stem cells, collagen I, and porous beta-tricalcium phosphate scaffolds Exp Biol Med 2013;238:1331–1343.

45. Temple JP, Hutton DL, Hung BP, Huri PY, Cook CA, Kondragunta R, Jia X, Grayson WL. Engineering anatomically shaped vascularized bone grafts with hASCs and 3D-printed PCL scaffolds. J Biomed Mater Res - A 2014;102:4317–4325. [PubMed: 24510413]

46. Laschke MW, Schank TE, Scheuer C, Kleer S, Schuler S, Metzger W, Eglin D, Alini M, Menger MD. Three-dimensional spheroids of adipose-derived mesenchymal stem cells are potent initiators of blood vessel formation in porous polyurethane scaffolds. Acta Biomater 2013;9:6876–6884. [PubMed: 23415749]

47. Fischer LJ, McIlhenny S, Tulenko T, Golesorkhi N, Zhang P, Larson R, Lombardi J, Shapiro I, DiMuzio PJ. Endothelial differentiation of adipose-derived stem cells: Effects of endothelial cell growth supplement and shear force. J Surg Res 2009;152:157–166. [PubMed: 19883577]

48. Laschke MW, Schank TE, Scheuer C, Kleer S, Shadmanov T, Eglin D, Alini M, Menger MD. In vitro osteogenic differentiation of adipose-derived mesenchymal stem cell spheroids impairs their in vivo vascularization capacity inside implanted porous polyurethane scaffolds. Acta Biomater 2014;10:4226–4235. [PubMed: 24998773]

49. Chung E, Rytlewski JA, Merchant AG, Dhada KS, Lewis EW, Suggs LJ. Fibrin-based 3D matrices induce angiogenic behavior of adipose-derived stem cells. Acta Biomater 2015;17:78–88. [PubMed: 25600400]

50. Rao RR, Peterson AW, Ceccarelli J, Putnam AJ, Stegemann JP. Matrix composition regulates three-dimensional network formation by endothelial cells and mesenchymal stem cells in collagen/fibrin materials. Angiogenesis 2012;15:253–264. [PubMed: 22382584]

51. Zhang X, Nan Y, Wang H, Chen J, Wang N, Xie J, Ma J, Wang Z. Model microgravity enhances endothelium differentiation of mesenchymal stem cells. Naturwissenschaften 2013;100:125–133. [PubMed: 23229853]

52. Duffy GP, Ahsan T, O'Brien T, Barry F, Nerem RM. Bone marrow-derived mesenchymal stem cells promote angiogenic processes in a time- and dose-Dependent manner in vitro. Tissue Eng - A 2009;15:2459–2470.

53. Holmes B, Bulusu K, Plesniak M, Zhang LG. A synergistic approach to the design, fabrication and evaluation of 3D printed micro and nano featured scaffolds for vascularized bone tissue repair. Nanotechnology 2016;27:064001. [PubMed: 26758780]

54. Saleh FA, Whyte M, Genever PG. Effects of endothelial cells on human mesenchymal stem cell activity in a three-dimensional in vitro model. Eur Cells Mater 2011;22:242–257.

55. Moon JJ, Saik JE, Poché RA, Leslie-Barbick JE, Lee SH, Smith AA, Dickinson ME, West JL. Biomimetic hydrogels with pro-angiogenic properties. Biomaterials 2010;31:3840–3847. [PubMed: 20185173]

56. Rohringer S, Hofbauer P, Schneider KH, Husa AM, Feichtinger G, Peterbauer-Scherb A, Redl H, Holnthoner W. Mechanisms of vasculogenesis in 3D fibrin matrices mediated by the interaction of adipose-derived stem cells and endothelial cells Angiogenesis 2014;17:921–933. [PubMed: 25086616]

57. Kim J, Kim HN, Lim KT, Kim Y, Pandey S, Garg P, Choung YH, Choung PH, Suh KY, Chung JH. Synergistic effects of nanotopography and co-culture with endothelial cells on osteogenesis of mesenchymal stem cells Biomaterials 2013;34:7257–7268. [PubMed: 23834896]

58. Meury T, Verrier S, Alini M. Human endothelial cells inhibit BMSC differentiation into mature osteoblasts in vitro by interfering with osterix expression. J Cell Biochem 2006;98:992–1006. [PubMed: 16479590]

59. Correia C, Grayson WL, Park M, Hutton D, Zhou B, Guo XE, Niklason L, Sousa RA, Reis RL, Vunjak-Novakovic G. In vitro model of vascularized bone: Synergizing vascular development and osteogenesis PLoS One 2011;6:e28352. [PubMed: 22164277]

60. McFadden TM, Duffy GP, Allen AB, Stevens HY, Schwarzmaier SM, Plesnila N, Murphy JM, Barry FP, Guldberg RE, O'Brien FJ. The delayed addition of human mesenchymal stem cells to preformed endothelial cell networks results in functional vascularization of a collagen-glycosaminoglycan scaffold in vivo. Acta Biomater 2013;9:9303–9316. [PubMed: 23958783]
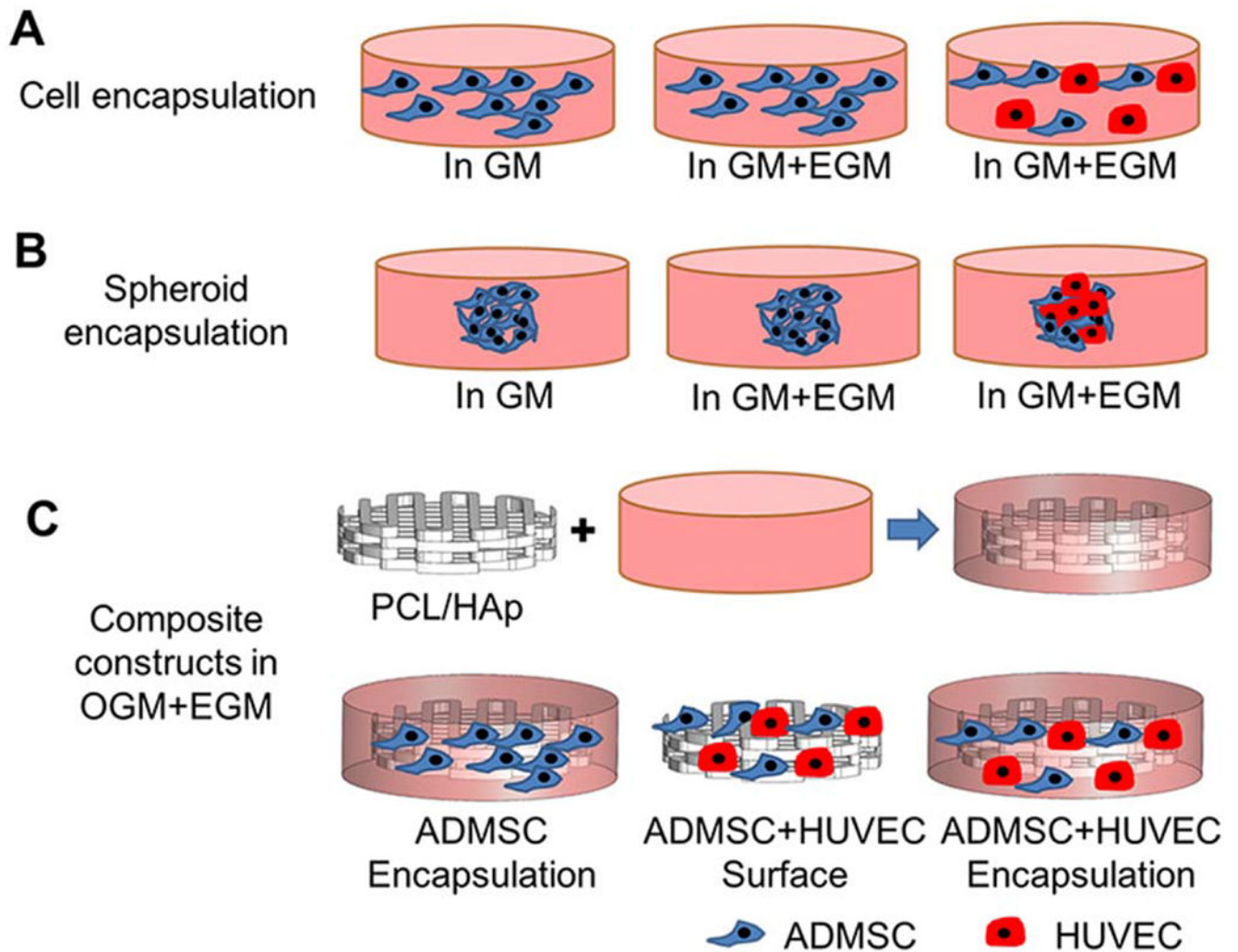
FIGURE 1.

Schematic of experimental design. (A) Homogeneous cell encapsulation within Me-HA/Me-Gel hydrogels: ADMSC or ADMSC-HUVEC and hydrogel precursors were loaded into silicone molds and subsequently exposed to 365 nm UV light for 60 s. The cell-hydrogel constructs were maintained in GM, hybrid media (GM and EGM) for 14 days; (B) Cellular spheroid encapsulation within hydrogels: ADMSC or ADMSC-HUVEC cell spheroids were fabricated first and then encapsulated within the hydrogels. The spheroid laden constructs were conditioned in GM or hybrid media for 7 days; (C) Composite constructs: PCL/HAp scaffolds were first 3D printed, then the printed scaffolds were incorporated with cell laden hydrogels. ADMSC or ADMSC-HUVEC were encapsulated. ADMSC-HUVEC were also surface seeded onto the printed PCL/Hap scaffolds. All of the constructs were conditioned in hybrid media with OGM and EGM for 21 days before further characterization or subcutaneous implantation.
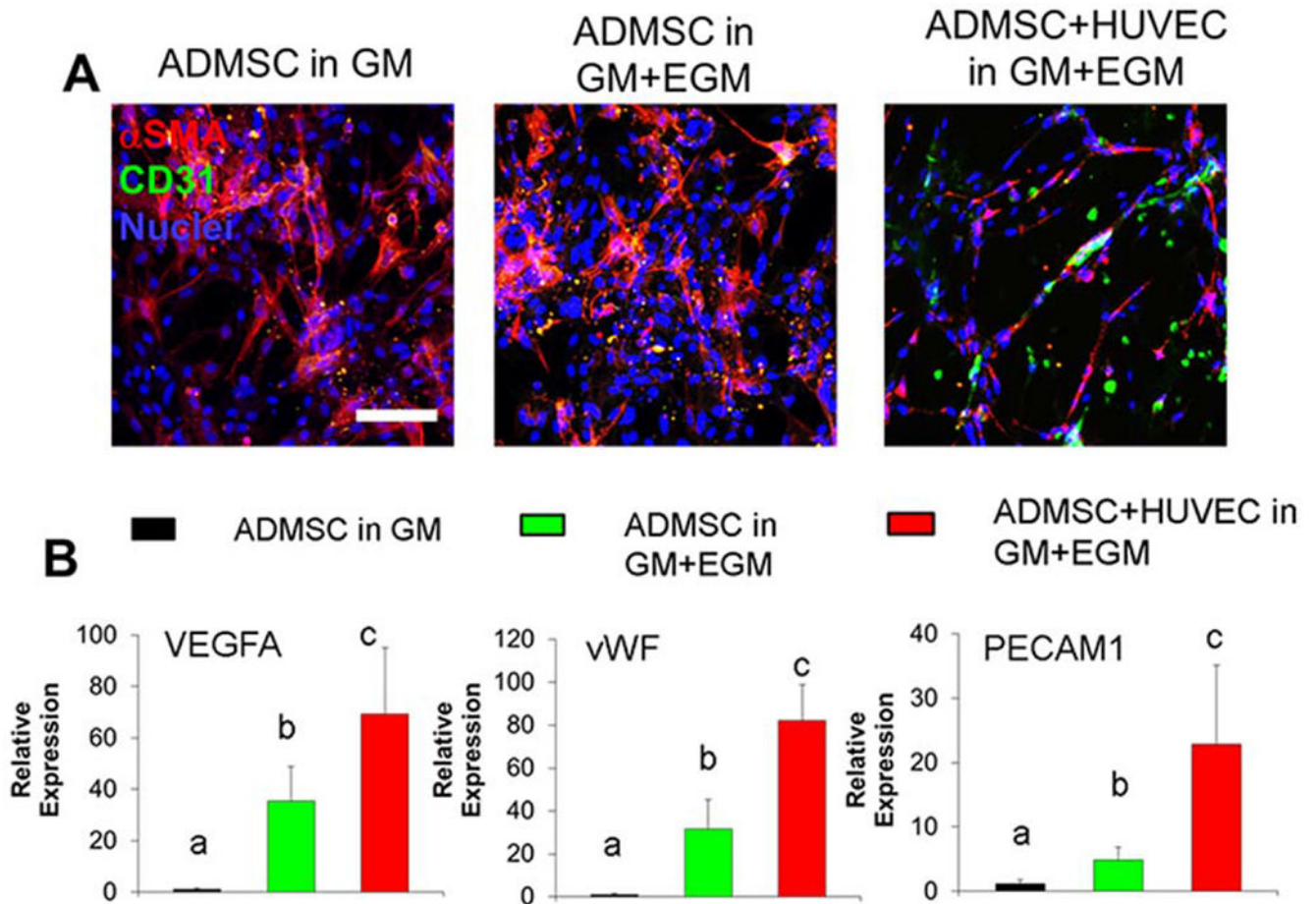
FIGURE 2.
3D Co-culture of ADMSC and HUVEC within the hydrogel promoted capillary network formation and vascularization gene expression. (A) Representative immunohistochemical (IHC) staining for αSMA (red), CD31 (green) and nuclei (blue) within cell laden hydrogels after 14-day culture; (B) qPCR analysis of VEGFA, vWF and PECAM1 in cell laden hydrogels after 14-day culture. Relative gene expression is presented as normalized to 18S and expressed relative to ADMSC in GM ($n = 3$; bars that do not share letters are significantly different from each other; $p < 0.05$). ADMSC or ADMSC-HUVEC were encapsulated and conditioned in GM or GM and EGM.
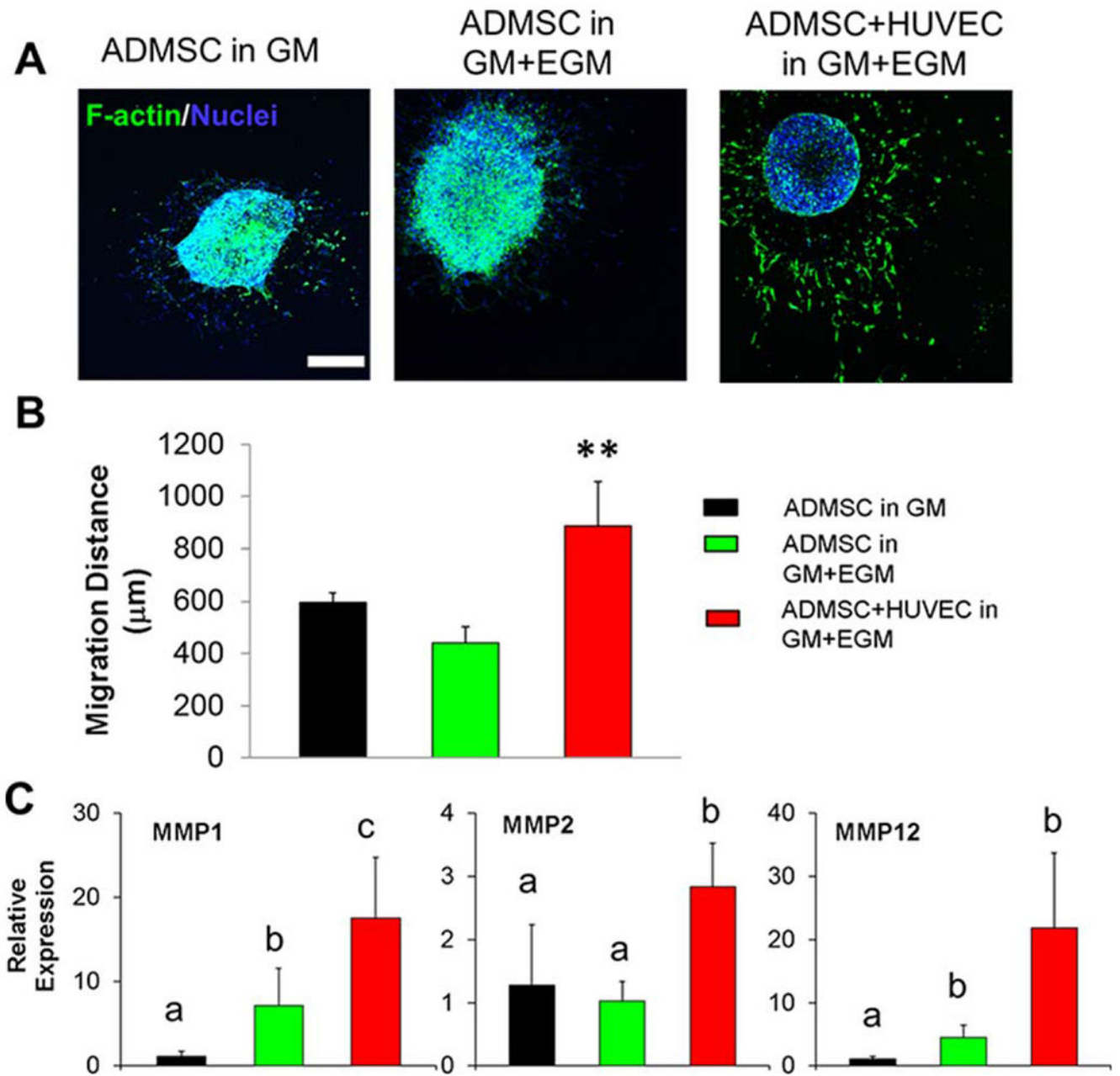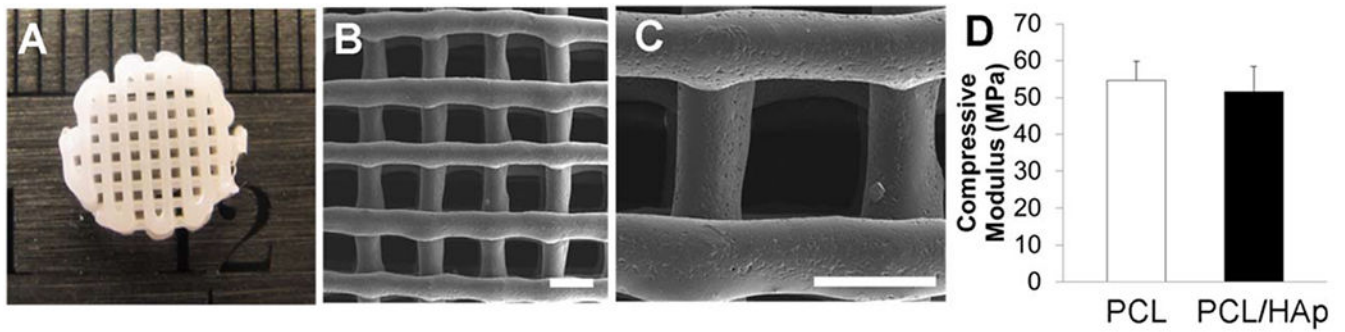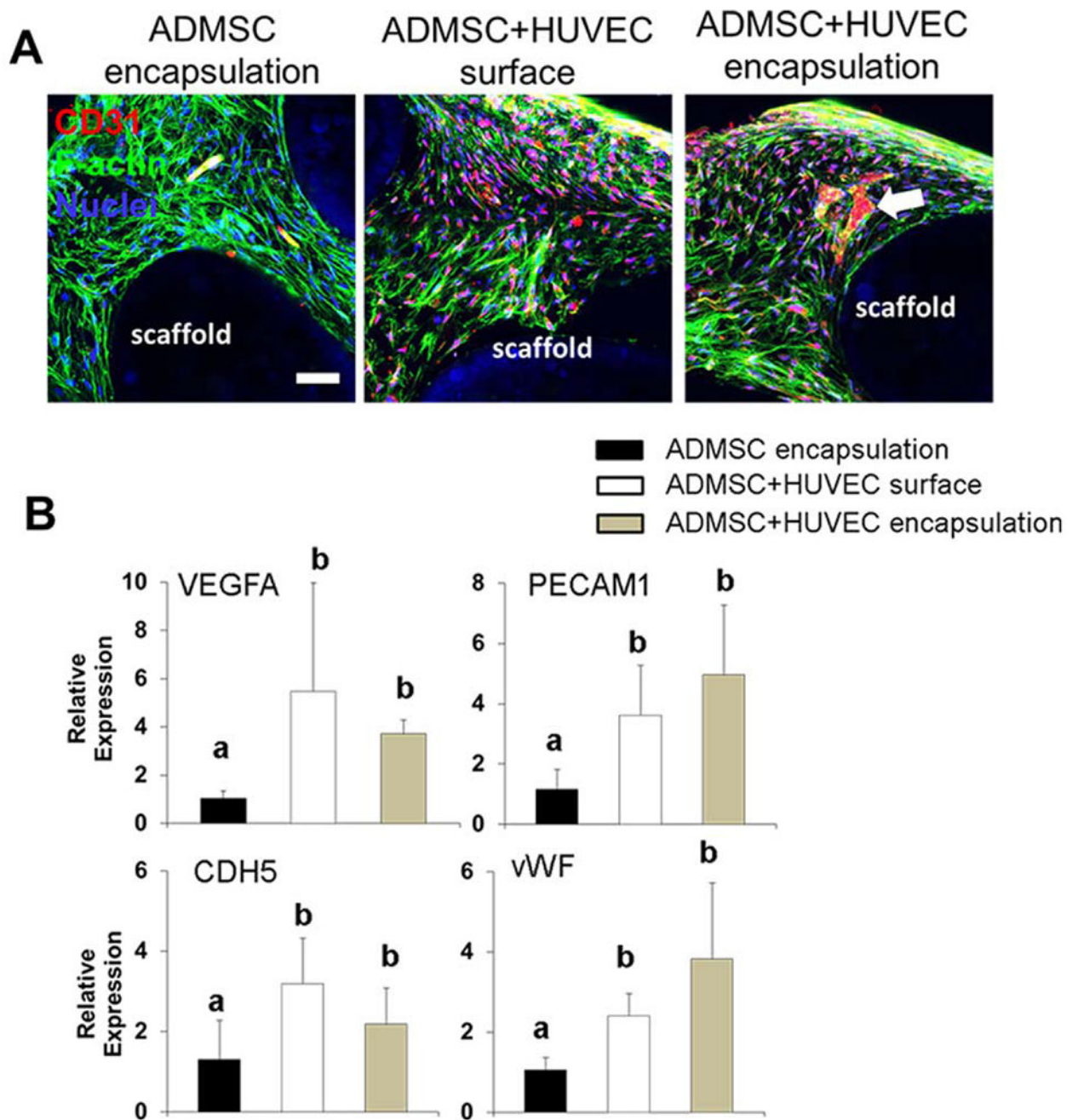
FIGURE 3.
3D co-culture of ADMSC and HUVEC spheroids within hydrogel promoted cell migration. (A) Representative images of phalloidin staining for F-actin (green) and nuclei (blue) within spheroid laden hydrogels after 7-day culture (scale bar: 500 μm); (B) cell migration distance from encapsulated spheroids (**$p < 0.01$); (C) qPCR analysis of MMP1, MMP2 and MMP12 in spheroid laden hydrogels after 7-day culture. Relative gene expression is presented as normalized to 18S and expressed relative to ADMSC in GM ($n = 3$; bars that do not share letters are significantly different from each other; $p < 0.05$). ADMSC or ADMSC-HUVEC spheroids were encapsulated and conditioned in GM or GM and EGM.

FIGURE 4.
3D printed PCL/HAp scaffold. (A) Representative image of 3D printed PCL/HAp scaffold with 10% of HAp nanocrystals; (B, C) SEM images of printed PCL/HAp scaffold (scale bar: 500 μm). The PCL/HAp scaffold had regular pores of around 500 μm and strands with a thickness of 350–450 μm; (D) Compressive modulus of 3D printed PCL and PCL/HAp scaffolds.

FIGURE 5.

In vitro vascularization within 3D printed scaffolds. (A) Representative IHC staining for F-actin (green), CD31 (red) and nuclei (blue) within cell laden hydrogels around 3D printed PCL/HAp scaffolds after 21-day culture (scale bar: 50 μm; white arrow indicates the formation of microvessel like structure); (B) qPCR analysis. Relative gene expression is presented as normalized to 18 S and expressed relative to scaffolds with ADMSC alone ($n = 3$; bars that do not share letters are significantly different from each other; $p < 0.05$).

ADMSC or ADMSC-HUVEC were encapsulated and conditioned in hybrid media with OGM and EGM.

FIGURE 6.
Co-culture of ADMSC and HUVEC within 3D printed scaffolds did not affect osteogenic differentiation *in vitro*. (A) Representative images for ALP staining after 21-day culture (scale bar: 1 mm); (B) ALP activity (**$p < 0.01$); (C) qPCR analysis. Relative gene expression is presented as normalized to 18S and expressed relative to scaffolds with ADMSC alone. ($n = 3$). ADMSC or ADMSC-HUVEC were encapsulated and conditioned in hybrid media with OGM and EGM.
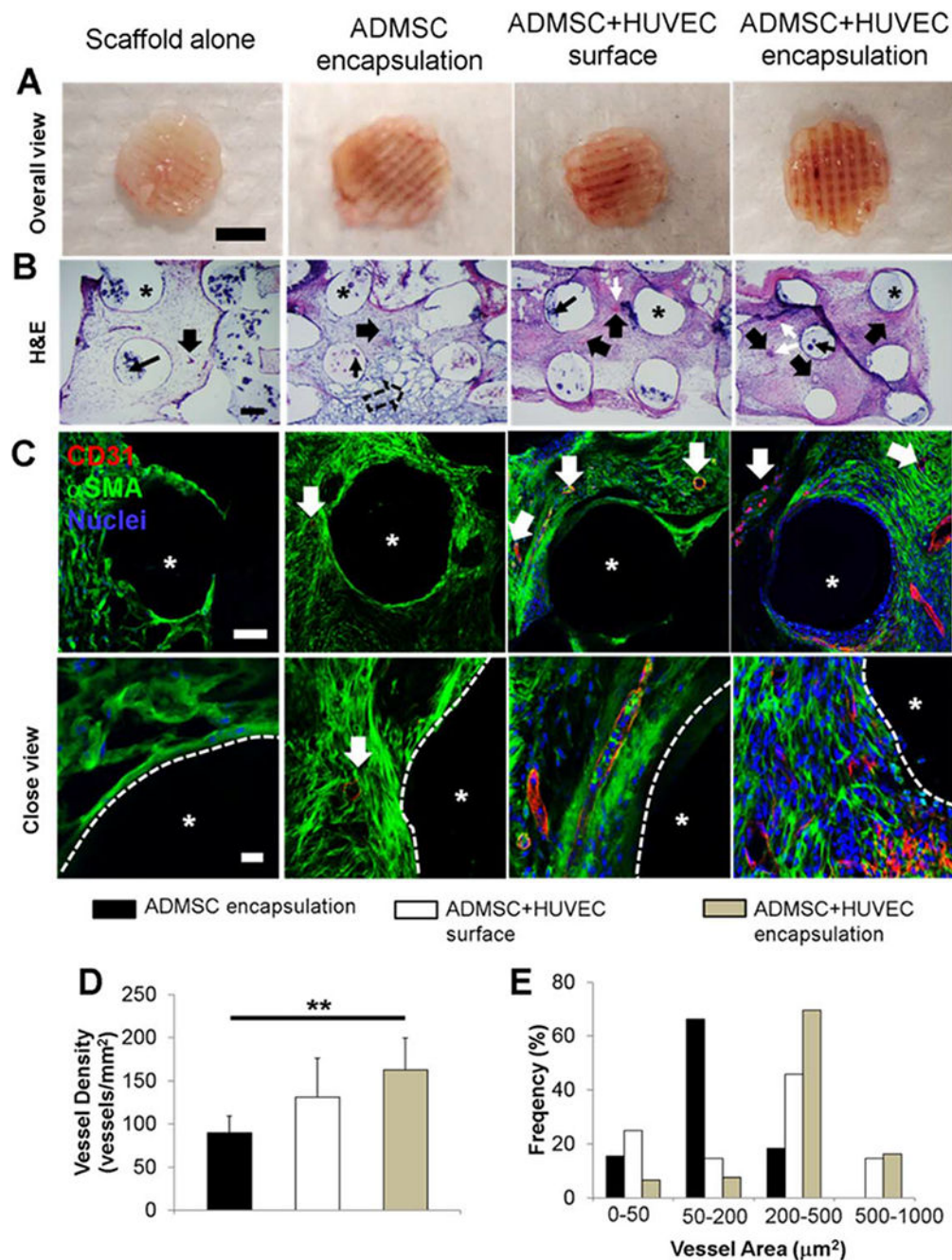
FIGURE 7.

In vivo vascularization within 3D printed scaffolds. (A) Overall view of explanted scaffolds after 4-week subcutaneous implantation (scale bar: 4 mm); (B) Representative images of H&E staining (scale bar: 200 μm). The wide, solid arrows indicate the formed microvessels with lumen structure and red blood cells inside. These microvessels can be of either human or mouse origin. The black, narrow arrows indicate the HAp particles. White, narrow arrows indicate the murine erythrocytes within blood vessels. The remnants of hydrogels are denoted by hollow arrow, and the asterisks indicate the PCL/HAp scaffold strand areas; (C)

IHC staining for human CD31 (red), αSMA (green), and nuclei (blue) within 3D printed scaffolds. The white, solid arrows indicate the stained cells/microvessles positive for human CD31. Very few human CD31 positive cells were observed in scaffold alone group, indicating that the formed capillaries were of mouse origin. The asterisks indicate the PCL/HAp scaffold strand areas; (D) Microvessel density of the scaffolds. The density was measured in vessels/mm^2. (**$p < 0.01$); (E) Microvessel area distribution in the scaffolds. The microvessel density and microvessel area distribution were measure by quantifying the formed CD31 positive vascular-network.